Geophys. J. R. astr. Soc. (1981) **66**, 553–578

Pleistocene deglaciation and the Earth's rotation: implications for mantle viscosity

R. Sabadini* and W. R. Peltier *Department of Physics, University of Toronto, Toronto, Ontario M5S 1A7, Canada*

Received 1980 October 27; in original form 1980 April 30

Summary. Recent results from the analysis of postglacial rebound data suggest that the viscosity of the Earth's mantle increases through the transition region. Models which fit both relative sea-level and free air gravity data have viscosities which increase from a value near 10^{22} poise in the upper mantle beneath the lithosphere to a value of about 10^{23} poise in the lower mantle. In this paper we analyse the effect of deglaciation upon the Earth's rotation and thereby show that the observed secular trend (polar wander) evident in the ILS–IPMS pole path, and measurements of the non-tidal acceleration of the length of day, are both consistent with the viscosity profile deduced from postglacial rebound. The two analyses are therefore mutually reinforcing.

1 Introduction

The traditional method which has been employed to estimate the viscosity of the planetary mantle is that based upon analysis of postglacial rebound data. These data constitute a memory of the planet's response to the massive deglaciation event which began *c.* 18 000 yr BP. Although it is not our purpose here to discuss such analyses in detail, it is important to appreciate the main results which have been obtained to date. These results are based upon inversion of the data using a global model (Peltier 1974, 1976; Peltier & Andrews 1976; Peltier, Farrell & Clark 1978) which accepts as input a complete deglaciation history and produces as output predictions of relative sea-level, free air gravity anomaly, or other observable signatures (e.g. surface tilt) of the response. Preliminary analysis of relative sea-level data with this model suggested that the viscosity was sensibly constant and equal to about 10^{22} poise (Peltier & Andrews 1976; Peltier *et al.* 1978) or that the rsl data were insensitive to viscosity increases at sufficiently great depth. When the rsl histories were augmented by free air gravity data from the Laurentide region, it was found (Peltier 1980; Wu & Peltier 1981a, b) that some increases of viscosity with depth was required in order to fit the 35–40 mgal negative anomaly over the central depression. These data seem to require a lower mantle viscosity which is somewhat less than 10^{23} poise.

Since knowledge of the variation of mantle viscosity with depth is an important ingredient in a very wide range of geodynamic models, particularly those for the mantle

*Present address: Istituto di Geofisica, via Irnerio 28, Università di Bologna, 40126 Bologna, Italy.

convective circulation (Peltier 1980), it is interesting to enquire as to whether there might be other geophysical observations, distinct from those pertaining to glacial isostasy itself, which could be employed to verify the validity of the inference from isostatic adjustment. As we will show here, a set of data which does provide such corroboration is that which concerns changes in the Earth's rotation which were forced by the same deglaciation event responsible for producing the observed rsl variations. That we should expect this event to produce substantial effects upon rotation, follows immediately from the fact that the masses of the major ice sheets (Laurentide, Fennoscandian) were on the order of 10^{22} g, as may be deduced from the observation (e.g. Shepard 1963) that their melting effected a global sea-level rise of approximately 80 m.

In Fig. 1 we show the main set of data with which the analysis in this paper is concerned. The top and bottom portions of the figure illustrate the polar motion in CIO coordinates (x-axis through Greenwich and y-axis along 90° W longitude) based upon the reduction of early ILS data by Vicente & Yumi (1969, 1970) as described in Dickman (1977). These polar motion data clearly show the 7 yr beat period associated with the superposition of the 12 month annual and 14 month Chandler periodicities. This oscillatory component is itself

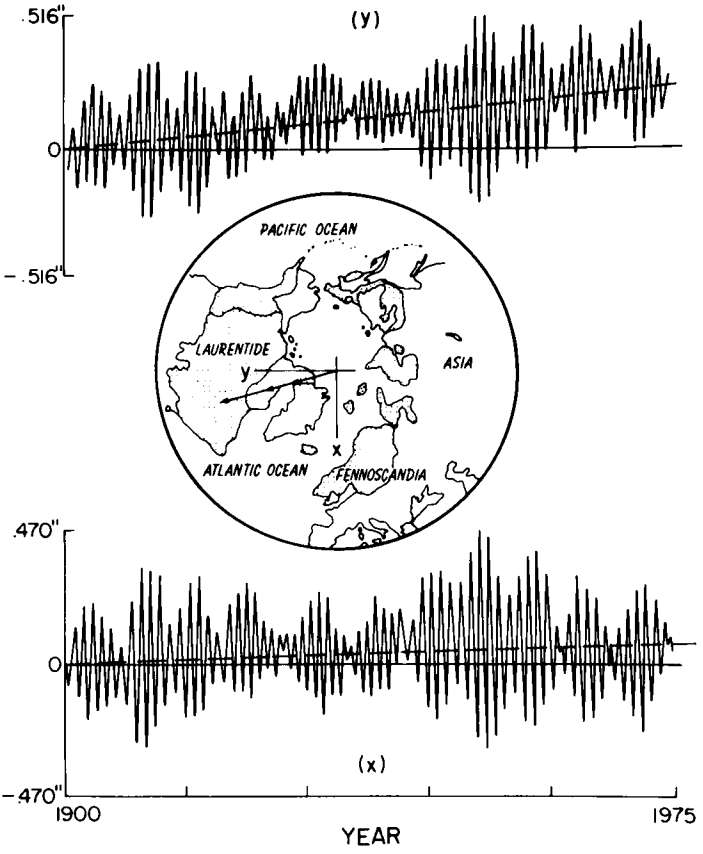

Figure 1. x and y components of the polar motion in CIO coordinates during the period 1900–75 based upon ILS–IPMS data. The dashed lines denote the secular trend upon which the 7 yr beat between the 14 month Chandler and 12 month annular variations are superimposed. This secular trend constitutes 'real' wander of the rotation pole relative to the geography. The inset polar projection shows the location of the CIO coordinates and the disposition with respect to them of the major continental ice sheets. The line extending from the origin of the CIO system and marked by the dark arrows denotes the current direction of polar wander.

superimposed upon a secular trend which constitutes real 'wander' of the rotation pole relative to the geographic coordinates. The slope of this secular trend is such as to imply a present day speed of polar wander of approximately $1^0/10^6$ yr. The direction of migration of the pole over the 75 yr period spanned by the polar motion data is shown in the central portion of Fig. 1 by the heavy arrow drawn from the origin of the CIO system.

Also shown in the central part of Fig. 1 are the locations of the major continental ice sheets which were in place at glacial maximum 20 000 yr ago. It is important for our purposes here to note that the direction of polar wander is approximately *towards* the ancient Laurentide ice sheet which was easily the largest of those which later disintegrated (Peltier & Andrews 1976). This is precisely what we would expect if the observed polar wander were induced by the deglaciation event: the net polar motion being in a direction determined by the vector sum of the forcing produced by the individual ice masses. Since the Laurentide sheet dominates the forcing we expect the polar wander to be very nearly in the direction of its centroid. The question which we shall address here is whether the observed rate of polar wander is compatible with the viscosity profile deduced from post-glacial rebound data and the known mass and areal extent of the major ice sheets.

In Section 2 we describe the simple theoretical model which we have developed for the purpose of analysing the above described polar motion data. Section 3 is concerned with a discussion of various exact and approximate methods which may be employed to solve the model equations and these are compared numerically. In Section 4 we first prove that a linear approximation to the complete system is adequate for most purposes and proceed to employ it to analyse the polar wander forced by deglaciation. From the observed speed of polar wander we infer a mean mantle viscosity. In Section 5 we employ the same model to predict a non-tidal variation in lod and show by fitting the model to this observation that the same viscosity is required as obtained from the analysis of polar wander. Our main conclusions are presented in Section 6.

2 A simple theoretical model

If we suppose that the Earth is subject to no external torque, then the principle of angular momentum conservation may be expressed in the form (e.g. Goldstein 1950)

$$\frac{d}{dt}(J_{ij}\omega_j) + \epsilon_{ijk}\,\omega_j J_{kl}\,\omega_l = 0, \tag{1}$$

which applies in a coordinate system rigidly attached to the Earth as a whole. This body fixed coordinate system, with its origin at the Earth's COM, is chosen such that the inertia tensor of the initially unperturbed Earth is diagonal. In (1), ω_i is the angular velocity vector, J_{ij} is the moment of inertia tensor, and ϵ_{ijk} is the Levi–Cevita (alternating) tensor. Munk & MacDonald (1960) remains an excellent reference to various applications of (1) to studies of the rotation of the Earth. The inertia tensor J_{ij} contains contributions from two sources which are of interest to us here, due respectively to the effect of the deformation produced by the basic rotation and that associated with the response of the planet to the surface loading of the ice sheets. Both of these effects are time-dependent but may be specified exactly if the rheology of the Earth and the deglaciation history may be assumed known. Because we are interested in testing the compatibility of the rotation data with postglacial rebound observations we will employ the same Maxwell model of the rheology as in Peltier (1974). In the remainder of this section we shall discuss the two contributions to J_{ij}. Once these are known, the problem of determining the rotational response of the Earth to deglaciation reduces to the problem of solving the set of simultaneous ordinary differential equations (1).

2.1 PERTURBATIONS OF INERTIA DUE TO VARIABLE ROTATION

The deformation of the Earth which is associated with its rotation may be determined most simply using the Love number formalism in combination with MacCullagh's formula (Jeffreys 1970). If the Earth is subject to a disturbing potential $\phi_2(r, s)$, such that

$$\phi_2(r, s) = \sum_{l=0}^{\infty} \Phi_{2,l}(r, s) P_l(\cos\theta) \tag{2}$$

where s is the Laplace transform variable, r the distance from the COM, and P_l the usual Legendre polynomial, then this applied potential will elicit a response $\phi_1(r, s)$ such that

$$\phi_{1,l}(r, s) = \Phi_{2,l}(r, s) k_l(r, s) \tag{3}$$

where $k_l(r, s)$ is the so called 'tidal' Love number. If the applied potential is the centrifugal potential Ψ associated with rotation, then

$$\Psi = \tfrac{1}{2}[\omega^2 r^2 - (\omega_i x_i)^2] \tag{4}$$

which (e.g. Munk & MacDonald 1960) can be split into two terms as

$$\Psi = \tfrac{1}{3}\omega^2 r^2 + \chi \tag{5}$$

where

$$\chi = \tfrac{1}{6}[\omega_1^2(x_2^2 + x_3^2 - 2x_1^2) + \ldots - 6\omega_1\omega_2 x_1 x_2] \tag{6}$$

is a spherical harmonic of degree 2 and the dots designate additional terms obtained by cyclic permutation of the indices. The external gravitational potential V, produced by this part of the centrifugal potential, therefore enters MacCullagh's formula as

$$V = \left(\frac{a}{r}\right)^5 \chi(t) * k_2(t) \tag{7}$$

where the $*$ indicates convolution (i.e. the Laplace inverse of (3)). The Love number $k_2(t)$ may be obtained from the equivalent time-independent expression for an elastic Earth (e.g. Munk & MacDonald 1960) by application of the correspondence principle (e.g. Peltier 1974). For an incompressible homogeneous Earth the elastic Love number is

$$k_2 = \frac{3/2}{1 + \bar{\mu}} \tag{8}$$

where $\bar{\mu} = 19\mu/2\rho g a$ is the non-dimensional rigidity in which μ is the elastic rigidity, ρ the density, g the surface gravitational acceleration, and a the radius of the homogeneous model. To apply the correspondence principle we simply note that $k_2(s)$ for the Maxwell model (Peltier 1974) is

$$k_2(s) = \frac{3/2}{1 + \bar{\mu}(s)}, \tag{9a}$$

where

$$\bar{\mu}(s) = \frac{\bar{\mu} s}{s + \mu/\nu}. \tag{9b}$$

The Laplace inverse of (9a) is

$$k_2(t) = \frac{3/2}{1 + \bar{\mu}}[\delta(t) + \bar{\mu}\gamma \exp(-\gamma t)], \tag{10}$$

where $\gamma = (\mu/\nu)/(1 + \bar{\mu})$ is the inverse relaxation time of the $l = 2$ component of the deformation in which ν is the molecular viscosity of the homogeneous model. Introducing the explicit expressions for ϕ and k_2 into MacCullagh's formula, we get

$$\frac{G}{2r^5}[C_{11}(x_2^2 + x_3^2 - 2x_1^2) + \ldots - 6C_{12}x_1x_2] = \left(\frac{a}{r}\right)^5 \chi(t) * k_2(t) \tag{11}$$

where $I\delta_{ij} + C_{ij}$ are the elements of the inertia tensor of the rotationally deformed sphere. Taking into account the fact that a solid harmonic will produce deformations which leave C_{ii} invariant (e.g. Rochester & Smylie 1974) we may equate similar terms on each side of (11) to obtain

$$C_{ij}(t) = \frac{a^5}{2G(1+\bar{\mu})}\left[\omega_i(t)\omega_j(t) - \frac{\omega^2(t)}{3}\delta_{ij} + \bar{\mu}\gamma\int_{-\infty}^{t}\left[\omega_i(t')\omega_j(t') - \frac{\omega^2(t')}{3}\delta_{ij}\right] \times \exp\left[-\gamma(t-t')\right]dt'\right]. \tag{12}$$

It is a consequence of the incompressibility of the model that the term $\omega^2 r^2/3$ in (5) does not contribute to the perturbations of inertia (Rochester & Smylie 1974). To obtain the total inertia of the rotating sphere we must add to (12) the inertia which exists in the absence of rotation. This may be obtained by assuming that the effect of rotation is to change the moment about the polar axis by $2\Delta/3$ and about the two orthogonal equatorial axes by $-\Delta/3$ (e.g. Burgers 1955) where Δ is unknown. If we insist that the resulting principal moments must equal the observed values C and A (say) we get the moment of inertia of the non-rotating sphere (I) as

$$I = A + \frac{C - A}{3}. \tag{13}$$

We may then write the total inertia tensor $J_{ij}(t)$ as

$$J_{ij}(t) = I\delta_{ij} + C_{ij}(t) + I_{ij}(t) \tag{14}$$

where $I_{ij}(t)$ is the variation of the inertia tensor which is forced by the surface mass loading of the ice sheet and the deformation of the Earth which is produced in response. In order to calculate this contribution we shall assume (reasonably) that variations in rotation do not feed back on to the rebound itself. We shall also assume that the earth model is homogeneous and incompressible as above. Since the rotational response to deglaciation is entirely associated with the $l = 2$ component of the load and of the response to it, and since the $l = 2$ deformation samples the entire mantle, any inference which we make by fitting the homogeneous model to the observations will refer to the *mean* material properties of the interior. Since the real Earth is neither incompressible nor homogeneous it is useful to adjust the parameters of the model to reflect reality better. Some improvement may be obtained if the fluid part of the k_2 Love number in (10) is forced to equal that which is observed the result being the so-called equivalent earth model (Munk & MacDonald 1960) in which

$$3/2 \to k_f \tag{15}$$

where $k_f = 0.96$.

2.2 PERTURBATIONS OF INERTIA DUE TO SURFACE MASS LOADING AND ISOSTATIC ADJUSTMENT

The contributions to I_{ij} in (14) are due to the ice sheets themselves and to the deformation which their melting induces. Rather than attempting to employ a detailed deglaciation model such as that described in Peltier & Andrews (1976), particularly since such models may still contain rather significant errors (Peltier 1980), we will use a simple spherical ice cap to model the glacial forcing. Since this forcing is so strongly dominated by the large Laurentide ice sheet, whose geometry is well known, we expect that the error incurred in employing such a simplified representation will be small. The strategy which we shall adopt for calculating I_{ij} in (14) is to obtain it in a coordinate system which has the ice cap on its polar axis and in this coordinate system we shall call the tensor components I'_{ij}. Having computed I'_{ij} in this fashion we may obtain I_{ij} by multiplying I'_{ij} with an appropriate rotation matrix. An ice sheet of angular radius α and total mass M may be described by the following surface density (Farrell 1972)

$$\sigma^{\mathrm{ICE}}(\theta) = \frac{M}{4\pi a^2}\left(P_0 + \sum_{l=1}^{\infty} \frac{(2l+1)(1+\cos\alpha)}{l(l+1)} \frac{\partial P_l(\cos\alpha)}{\partial \cos\alpha} P_l(\cos\theta)\right) \tag{16}$$

where θ is the angular distance from the centre of the ice cap. We may force our system to mimic a closed hydrological cycle by assuming that there is a defect of mass in a global ocean outside the ice sheet of magnitude $-M$ distributed over the surface area $2\pi a^2(1 + \cos\alpha)$ and thus corresponding to the surface density

$$\sigma^{\mathrm{OC}}(\theta) = \frac{M}{4\pi a^2}\left(-P_0 + \sum_{l=1}^{\infty} \frac{(2l+1)(1-\cos\alpha)}{l(l+1)} \frac{\partial P_l(\cos\alpha)}{\partial \cos\alpha} P_l(\cos\theta)\right). \tag{17}$$

Conservation of mass is then ensured by the fact that $\sigma_0^{\mathrm{OC}} + \sigma_0^{\mathrm{ICE}} = 0$ (i.e. the $l = 0$ components cancel).

In the coordinate system $Ox'_1x'_2x'_3$, in which the centre of the ice cap lies along the x'_3-axis and distance a from the origin, the perturbations of inertia due to the surface mass distribution $\sigma(\theta) = \sigma^{\mathrm{OC}}(\theta) + \sigma^{\mathrm{ICE}}(\theta)$ can be written as

$$I'_{11} = \frac{a^2}{3} L_2 \tag{18a}$$

$$I'_{22} = I'_{11} \tag{18b}$$

$$I'_{33} = -2I'_{11} \tag{18c}$$

where

$$L_2 = \int_0^{2\pi}\int_{-1}^{+1} P_2(x)\sigma(x,\phi)a^2\,dx\,d\phi \tag{19}$$

and the off-diagonal elements of I'_{ij} are identically zero. In general σ (and thus L_2) is time-dependent and it is through this dependence that we shall later introduce explicit deglaciation histories into the model. In the Laplace transform domain this requires $\sigma = \sigma(s)$.

The contribution to I'_{ij} due to isostatic compensation is produced by the change in shape of the planet as a whole which is effected by viscous flow due to the initial isostatic disequilibrium. This contribution may be calculated as follows. By definition the inertia tensor I'_{ij} is

$$I'_{ij} = \int_v \rho(x'_l x'_l \delta_{ij} - x'_i x'_j)\,dv \tag{20}$$

where $\mathbf{x}'(\mathbf{x}, s)$ denotes the position vector of the mass element with density ρ in the reference frame $Ox_1'x_2'x_3'$ of the material particle $\mathbf{x}$ and may be expressed as

$$x_i' = x_i + u_i(\mathbf{x}, s). \tag{21}$$

Substituting (21) in (20) and linearizing with $\rho = \rho_0$ (homogeneous) yields

$$I_{ij}' = \rho_0 \int_v (x_l x_l \delta_{ij} - x_i x_j)\, dv + \rho_0 \int_v (2x_l u_l \delta_{ij} - x_l u_j - u_i x_j)\, dv \tag{22}$$

in which the first term is just the inertia of the unperturbed sphere, while the second gives the inertia due to the deformation induced by the load. Again due to incompressibility we have $I_{11}' = I_{22}'$ and $I_{33}' = -2I_{11}'$ so that it suffices to compute but one of the diagonal components.

To evaluate the second term in (22) for a disc load we require the displacement vector $\mathbf{u} = u_r \hat{e}_r + u_\theta \hat{e}_\theta$ which from Peltier (1974) may be written in the form

$$\mathbf{u}(s) = \sum_{l=0}^{\infty} \left(U_l(r, s) P_l(\cos\theta)\, \hat{e}_r + V_l(r, s) \frac{\partial P_l(\cos\theta)}{\partial\theta} \hat{e}_\theta \right). \tag{23}$$

Substituting (23) into the second term of (22), evaluated for I_{33}', gives

$$I_{33}'(s) = 2\rho_0 \int_0^a \int_0^{2\pi} \int_0^{\pi} r^3 [u_r(\theta, r, s) \sin^2\theta + u_\theta(\theta, r, s) \sin\theta \cos\theta] \sin\theta\, d\theta\, d\phi\, dr. \tag{24}$$

Now u_r and u_θ, for a load of arbitrary surface mass density σ may be obtained by convolution as (Peltier & Andrews 1976)

$$u_r(\theta, \phi, r, s) = \int_0^{2\pi} \int_0^{\pi} G^{\mathrm{R}}(\beta, r, s) \sigma(\theta', \phi', s) a^2 \sin\theta'\, d\theta'\, d\phi' \tag{25}$$

$$u_\theta(\theta, \phi, r, s) = \int_0^{2\pi} \int_0^{\pi} G^{\mathrm{T}}(\beta, r, s) \sigma(\theta', \phi', s) a^2 \sin\theta'\, d\theta'\, d\phi' \tag{26}$$

where G^{R} and G^{T} are the Green functions for radial and tangential displacement respectively, which give the impulse response of the system to a point mass load (Peltier 1974), and $\beta = \theta - \theta'$ denotes the angular separation between the point of observation and the point of application of the load. Since G^{R} and G^{T} have spherical harmonic decompositions

$$G^{\mathrm{R}}(\theta, r, s) = \sum_{l=0}^{\infty} G_l^{\mathrm{R}}(r, s) P_l(\cos\theta), \tag{27}$$

$$G^{\mathrm{T}}(\theta, r, s) = \sum_{l=0}^{\infty} G_l^{\mathrm{T}}(r, s) \frac{\partial P_l(\cos\theta)}{\partial\theta}, \tag{28}$$

substitution of (27) and (28) in (24), making use of the addition theorem for spherical harmonics and the implications of the incompressibility condition, yields

$$I_{33}'(s) = \frac{-16\pi\rho_0}{5} \int_0^a \int_0^{2\pi} \int_{-1}^{+1} r^3 \left(\frac{G_2^{\mathrm{R}}(r, s)}{3} + G_2^{\mathrm{T}}(r, s) \right) P_2(x') a^2 \sigma(x', \phi', s)\, dx'\, d\phi'\, dr. \tag{29}$$

For the incompressible sphere the parameters G_2^R, G_2^T are given explicitly by (Wu & Peltier 1980a)

$$G_2^R = \frac{1}{\epsilon + \mu\delta}(d_1 r^3 + d_2 r)\left(1 + \frac{\bar{\mu}\gamma}{s+\gamma}\right) \tag{30a}$$

$$G_2^T = \frac{1}{\epsilon + \mu\delta}\left(\frac{5}{6} d_1 r^3 + \frac{d_2 r}{2}\right)\left(1 + \frac{\bar{\mu}\gamma}{s+\gamma}\right), \tag{30b}$$

where $\epsilon = 8\pi G\rho_0^2/3$, $\delta = 19/a^2$, $d_1 = 2G\rho_0/a^5$, $d_2 = -16G\rho_0/3a^3$.

Substitution of (30) into (29) leads to the analytic result

$$I'_{33}(s) = \frac{-8\pi\rho_0}{15} a^5 \left(\frac{d_1 a^2 + d_2}{\epsilon + \mu\delta}\right)\left(1 + \frac{\bar{\mu}\gamma}{s+\gamma}\right) L_2(s) \tag{31}$$

where $L_2(s)$ is as defined in (19). Incompressibility requires $I'_{22} = I'_{11}$ and $I'_{11} = -I'_{33}/2$, as previously.

These perturbations to the inertia tensor due to global relaxation under the ice sheet may be expressed in terms of the surface load Love number $k_2^L(s)$. In fact, the instantaneous elastic part of $k_2^L(s)$ is just

$$k_2^L = \frac{3}{5} \cdot \frac{M_e}{\epsilon + \mu\delta}(d_1 a^2 + d_2) \tag{32}$$

so that application of the correspondence principle yields

$$k_2^L(s) = k_2^L\left(1 + \frac{\bar{\mu}\gamma}{s+\gamma}\right) \tag{33}$$

and the component of the inertia perturbation I'_{33} in (31) may then be written

$$I'_{33}(s) = -\frac{2}{3} a^2 L_2(s) k_2^L(s). \tag{34}$$

Combining (34) (using $I'_{11} = -I'_{33}/2$) with (18a) gives (with $L_2(s) = L_2 \cdot f(s)$ in which L_2 is obtained from (19) and $f(s)$ contains the s dependence of the load)

$$I'_{11}(s) = \frac{a^2 L_2}{3}[1 + k_2^L(s)] f(s). \tag{35}$$

The Love number k_2^L must be corrected to take into account both the inhomogeneity of the real Earth and the sinking of the surface load. This correction is obtained by making use of the isostatic factor l to correct the elastic part of k_2^L in equation (34) as

$$k_2^L = -\frac{1-l}{1+\bar{\mu}} \tag{36}$$

where $l = 4(b/a) \cdot (1 - \rho'/\rho_0)$ (Munk & MacDonald 1960). In this expression b is the average crustal thickness, and ρ' the average density of the crust. When the complete tensor I'_{ij} is rotated counter-clockwise through the angle θ about the y-axis, where θ is the colatitude of the centre of the ice sheet, and the result transformed into the time domain by explicit calculation of the Laplace inverse, the result is the tensor $I_{ij}(t)$ which appears on the right side of (14) for $J_{ij}(t)$, which is itself required in the system (1).

3 Solution for the forced rotational response: exact and approximate methods

Clearly the system of equations (1), with $J_{ij}(t)$ a known function (14) of the components of instantaneous angular velocity ω_i and the applied load, are highly non-linear in general and therefore difficult to solve. In this section we shall establish the conditions under which the general system (1) may be approximated by an equivalent linear system by investigating the rotational response of the earth model to a specific (and simple) deglaciation history. Exact and approximate methods of solution will be discussed in turn.

3.1 AN EXACT METHOD OF SOLUTION FOR HEAVISIDE EXCITATION

Suppose that the planet has been spinning with angular velocity Ω about its axis of greatest inertia from $t = -\infty$ until $t = 0$, at which time it is perturbed by the addition to its surface of the circular ice cap described in Section 2.2. We shall assume that this ice cap remains on the surface thereafter. With the change of variable

$$m_i = \frac{\omega_i}{\Omega}, \tag{37}$$

where the m_i are the direction cosines of the rotation axis in the $Ox_1x_2x_3$ coordinate system, the $C_{ij}(t)$ defined in (12) may be simplified by evaluating the integrals analytically for $t \in [-\infty, 0]$ to give

$$C_{ij}m_j = \frac{a^5\Omega^2 k_f}{3G(1+\bar{\mu})}\left[\frac{2}{3}m_j m_j m_i + \bar{\mu}\exp(-\gamma t)m_3\delta_{3i} - \frac{\bar{\mu}}{3}\exp(-\gamma t)m_i\right.$$
$$\left. + \bar{\mu}\gamma m_j\int_0^t m_i m_j \exp[-\gamma(t-t')]dt' - \frac{\bar{\mu}\gamma}{3}m_i\int_0^t m_k m_k \exp[-\gamma(t-t')]dt'\right] \tag{38}$$

and in the following we shall define the constant $R = a^5\Omega^2 k_f/3G(1+\bar{\mu})$. Now the set of equations (1) constitutes a system of three coupled non-linear integro-differential equations because of the appearance of the history integrals in (38). By defining the auxilliary variables

$$h_{ij} = \gamma\int_0^t m_i m_j \exp[-\gamma(t-t')]dt' \tag{39}$$

this system may be reduced to an equivalent set of ordinary differential equations which may be solved as an initial value problem using conventional methods. Because the h_{ij} matrix is symmetric it has only six independent elements. If these independent elements are assembled with the m_i into a 9-vector $\mathbf{y} = (m_1, m_2, m_3, h_{11}, h_{22}, h_{33}, h_{12}, h_{13}, h_{23})$, then the system of equations (1) may be written in matrix form as

$$\begin{bmatrix}\mathbf{A}^*(x) & 0\\ 0 & \mathbf{I}\end{bmatrix}\frac{d\mathbf{y}}{dx} = \begin{bmatrix}\mathbf{B}^*(x) & 0\\ 0 & \mathbf{D}\end{bmatrix}\mathbf{y} \tag{40}$$

where x is a non-dimensional time defined as

$$x = \frac{\Omega R\bar{\mu}t}{I} \tag{41}$$

and where we have initially neglected the contribution to $J_{ij}(t)$ due to the ice load and the deformation associated with it. The factor $\Omega R\bar{\mu}/I$ in (41) has the dimensions of inverse time

and is in fact the initial frequency of the Chandler wobble forced by the glaciation event. In (40) the matrices $\mathbf{A}^*(x)$ and $\mathbf{B}^*(x)$ are 3×3, $\mathbf{I}$ is the 6×6 identity matrix, and $\mathbf{D}$ is 6×9. The elements of each of these matrices are given in Appendix A.

If the effect due to the surface load alone were included in (1), as described by $I_{ij}(t)$ in (14), and the $C_{ij}(t)$ and $I\delta_{ij}$ neglected, then (1) would reduce to the system

$$\mathbf{P}\frac{d\mathbf{m}}{dx} = \mathbf{Q}\mathbf{m} \tag{42}$$

where $\mathbf{P}$ and $\mathbf{Q}$ are 3×3 matrices whose non-dimensional forms are given in Appendix B for Heaviside excitation. When both the effects of loading and of rotation are included, as they must be in the full problem, then the evolution of the system is described by (40) with $\mathbf{A}^*(x)$ replaced by $\mathbf{A} = \mathbf{A}^* + \mathbf{P}$ and $\mathbf{B}^*(x)$ replaced by $\mathbf{B}(x) = \mathbf{B}^* + \mathbf{Q}$. The resulting set of simultaneous ordinary differential equations may therefore be written in standard form as

$$\frac{d\mathbf{y}}{dx} = \begin{bmatrix} \mathbf{A}^{-1} & \mathbf{B} & 0 \\ & \mathbf{D} & \end{bmatrix}\mathbf{y}. \tag{43}$$

This system may be solved using standard numerical procedures, but before presenting such solutions we will first describe two approximate methods of solution with which the exact solution will be compared.

3.2 APPROXIMATION SCHEMES

The first approximation scheme which we shall consider is that proposed by Munk & MacDonald (1960) for application to the problem of polar wander under conditions such that the axes of figure and rotation do not wander too far from the reference pole. The set of equations (1) is linearized in the quantities m_i and I_{ij}/C and the result, in the Laplace transform domain of the imaginary frequency s, is the algebraic system

$$\left(\frac{i}{\sigma_r}s + 1\right)m(s) = \Psi_D(s) + \phi(s) \tag{44}$$

where $\sigma_r = \Omega(C-A)/A$ is the Chandler wobble frequency for a rigid earth and where $m(s)$ is the complex variable $m(s) = m_1(s) + im_2(s)$ in which m_1 and m_2 are the direction cosines of the rotation axis in the $Ox_1x_2x_3$ system and $\Psi_D(s)$ and $\phi(s)$ are respectively the excitation functions due to the rotational deformation and surface load. The latter have the explicit forms

$$\Psi_D(s) = \frac{k_2(s)}{k_f}m(s) \tag{45a}$$

$$\phi_1(s) = \frac{I_{13}(s)}{C-A} + \frac{[sI_{23}(s) - I_{23}(0)]}{\Omega(C-A)} \tag{45b}$$

$$\phi_2(s) = \frac{I_{23}(s)}{C-A} - \frac{[sI_{13}(s) - I_{13}(0)]}{\Omega(C-A)} \tag{45c}$$

where $\phi(s) = \phi_1(s) + i\phi_2(s)$. In this scheme variations in the lod, which are described through $m_3(t)$, are decoupled from the m_1 and m_2 variations and may be calculated from $\phi_3(s)$ where

$$\phi_3(s) = \frac{-I_{33}(s)}{C}. \tag{46}$$

When explicit use is made of equations (10) and (15) in the expression for $\Psi_D(s)$ in (45a), then (44) has the simple s-domain solution

$$m(s) = \frac{-i\sigma_r}{\gamma - i\sigma_0}\left(\frac{\gamma}{s} - \frac{i\sigma_0}{s + \gamma - i\sigma_0}\right)\phi(s) \tag{47}$$

in which $\sigma_0 = \sigma_r\bar{\mu}/(1 + \bar{\mu})$ is the Chandler frequency for the Maxwell earth. From (47) it is apparent that, within the context of this linear approximation, the problem consists simply of a discussion of the extent to which two normal modes are excited by the deglaciation forcing. These two normal modes correspond respectively to the poles at $s = 0$ and at $s = i\sigma_0 - \gamma$ in the complex s-plane. The first of these, at $s = 0$, contains the polar wander component of the response while the second is just the free Eulerian nutation (Chandler wobble) which is damped at the rate γ due to the imperfection of elasticity embodied in the Maxwell rheology. In general the deglaciation event will excite both wander and wobble although the strength of the forcing at the Chandler frequency will be extremely weak if the time-scale of deglaciation is sufficiently long. Obviously we would prefer to employ the simple linear solution (47), rather than the exact solution embodied in (43), but before doing so we are obliged to establish its accuracy.

A second approximation scheme which we shall also discuss briefly was proposed by Burgers (1955) for a model with standard linear solid rheology rather than for the Maxwell rheology which is most appropriate to the problem of polar wander which concerns us here. Burgers' approximation is less restrictive than complete linearization, and is based upon the assumption that the Earth behaves as a perfect fluid in so far as the rotation is concerned. This assumption suffices to filter the Chandler mode completely from the dynamical system which is the reason for its theoretical utility. The same approximation was employed in Munk & MacDonald (1960) to solve the so-called Goguel–Fermi problem and is embodied in their equations (12.6.3) which in the present application take the form

$$\frac{dm_1}{dx'} = S_1 - \Gamma S_2 m_3 + \Gamma S_3 m_2 \tag{48a}$$

$$\frac{dm_2}{dx'} = S_2 + \Gamma S_1 m_3 - \Gamma S_3 m_1 \tag{48b}$$

$$\frac{dm_3}{dx'} = S_3 - \Gamma S_1 m_2 + \Gamma S_2 m_1 \tag{48c}$$

in which the quantities Γ, S_1, S_2, S_3, are defined in Appendix C for the case in which the load has a Heaviside time dependence and with $x' = t/\text{SCALE}$ where the time-scale SCALE is taken somewhat arbitrarily to be 10^3yr. Like the complete system (43) the approximate system (48) may be solved as an initial value problem using a standard subroutine for the solution of simultaneous ode's. In the following subsection we shall compare exact and approximate solutions for the Heaviside load history.

3.3 COMPARISON OF EXACT AND APPROXIMATE SOLUTIONS

In the limit of small time following application of the load, the linear solution (47) is exact and so may be employed to compute starting values for the non-linear systems (43) and (48). Given the starting values, these systems of ode's may be integrated directly and for this purpose we have employed the sixth-order accurate Runge–Kutta–Fehlberg scheme

Table 1.

Parameter	Symbol	Value
Viscosity	ν	10^{22} poise
Ice sheet mass	M	2×10^{20} kg
Angular radius of ice sheet	α	15°
Initial displacement of the centre of the ice sheet from the axis of figure	θ	25°
Density	ρ_0	5517 kg m^{-3}
Rigidity	μ	1.4519×10^{11} N m^{-2}
Gravitational acceleration	g	9.82 m s^{-2}
Earth's radius	a	6.371×10^{6} m
Earth's mass	M_e	5.976×10^{24} kg
Crust thickness	b	20 km
Crust average density	ρ'	2840 kg m^{-3}

described by Enright & Hull (1976). Although the direct integration of (48) is straightforward, the same is not true for the exact equation (43). The difficulty with (43) is due to the fact that it contains two widely separated time-scales due to the Chandler wobble and polar wander components of the response. The short time-scale wobble component is filtered in (48) but its presence in (43) makes the system 'stiff' and obliges us to employ a short time-step based on the Chandler period which means that direct integration requires considerable CPU time. In practise we sample the response approximately 10 times per cycle and extract the polar wander by applying a running average to the complete history.

In Table 1 we list the model parameters to be employed in the following comparisons of exact and approximate solutions for the response due to a Heaviside glaciation history. Several of the quantities listed in the table, such as the viscosity of the mantle and the ice sheet radius and mass, are employed only for illustrative purposes in this section.

Figs 2 and 3 compare the exact and two approximate solutions for the polar wander forced by a Heaviside excitation. Only the secular variation in m_1 is shown (since all of the

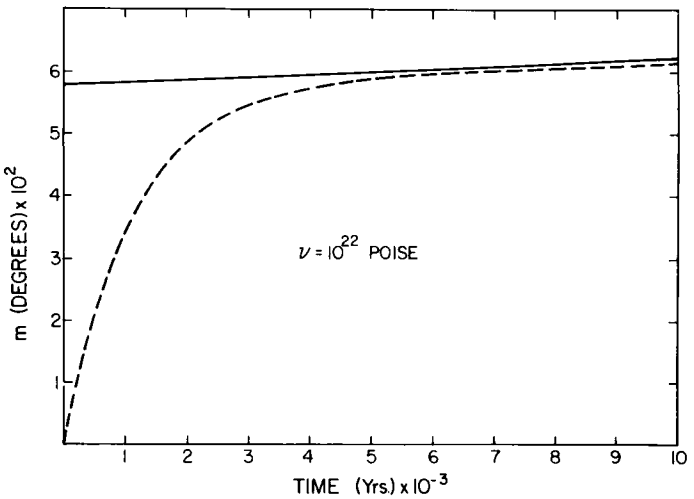

Figure 2. Comparison between exact and approximate solutions for polar wander forced by a Heaviside loading history, i.e. the spherical ice cap accretes instantaneously at $t = 0$ and remains in place for all time thereafter. The solid line (——) is the approximate solution, obtained using equations (48). The dashed line (– – –) is the exact solution obtained using equation (43) and the linear approximation based upon equation (47).

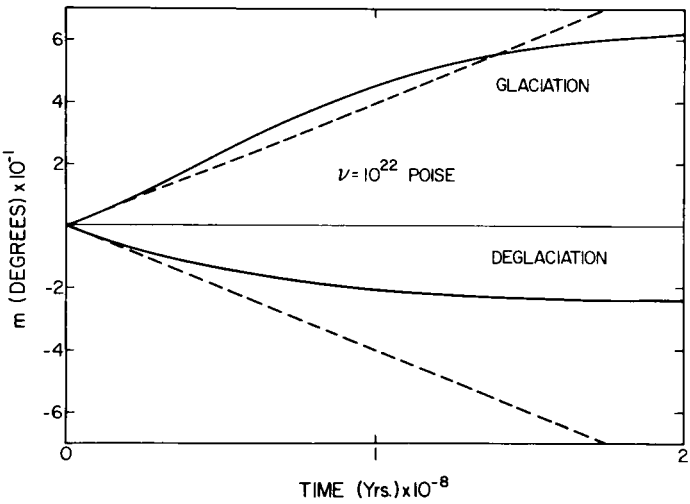

Figure 3. Complete polar wander history forced by loading due to sudden application of a circular ice cap for both positive loading (glaciation) and negative loading (deglaciation). In each case the centre of the circular ice cap is 25° away from the initial position of the rotation pole. The solid line is the exact solution and the dashed line the linear approximation.

time-dependence of m_2 is due to Chandler wobble) and variations of m_3 will be discussed later in relation to the question of the forced variations of lod. The linear solution, shown as the broken line on Fig. 3, is obtained from the Laplace inverse of (47) which gives

$$m_1(t) = \frac{\Omega}{A\sigma_0}\{\gamma P_1(1+\bar{\mu})t + (P_1+P_2)[\![1 - \exp[(-\gamma + i\sigma_0)]t]\!]\} \tag{49}$$

where $P_1 = \cos\theta \sin\theta L_2 a^2 \mathscr{L}/(1+\bar{\mu})$, $P_2 = \cos\theta \sin\theta L_2 \bar{\mu} a^2/(1+\bar{\mu})$, and we have used $f(s) = 1/s$ in the definition of $\phi(s)$ in (47) since the load history is a step function in time. Inspection of Fig. 3 shows that the polar wander part of the linear solution begins to deviate substantially from the exact solution (solid line) for times in excess of some tens of millions of years. In Fig. 2 the linear solution (dashed line) coincides with the exact solution while the approximate solution obtained from (48) (solid line), on the other hand, becomes a good approximation to the history only after the Chandler wobble has been damped significantly.

In Fig. 3 we have employed the long-term accuracy of the system (48) to continue the exact solution from (43) beginning from a time $t = 4\gamma^{-1}$ until equilibrium is achieved. The curve labelled 'glaciation', in which m_1 takes on positive values due to our choice of π for the longitude of the centre of the ice cap, shows the polar wander produced by adding a positive load to the surface at $t = 0$ of radius α and by simultaneously removing an equivalent mass from the global ocean (the centre of the ice sheet is offset by 25° from the initial rotation axis). The equilibrium configuration in this case has the rotation pole displaced 65° away from the centre of the ice sheet. The second curve in Fig. 3, labelled deglaciation, shows the response to removal of an equivalent load within the same area of radius α and simultaneously adding the same mass to the global ocean. In equilibrium the new rotation pole coincides with the centre of the defect of mass, i.e. orthogonal to the final location of the pole in the glaciation case. In each case, the final location of the pole coincides with the axis of greatest inertia. The relaxation time of the polar wander in both cases, when the mantle viscosity is 10^{22} poise, is on the order of 10^8yr. This true polar wander is entirely a consequence of the non-zero value of the isostatic factor I in equation (36).

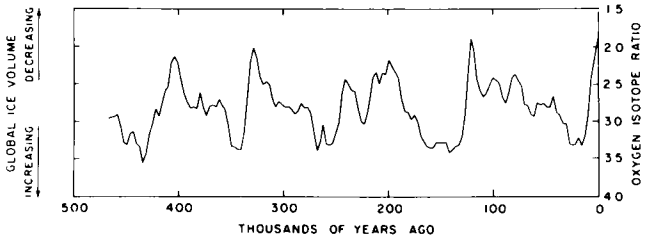

Figure 4. Oxygen isotope ratio (^{16}O, ^{18}O) variability obtained from a deep sea core covering the time period $0-5 \times 10^5$yr before present. These data are related to global ice volume in the manner shown and demonstrate that the long time-scale climatic fluctuations are dominated by quasi-periodic changes on a time-scale of 10^5yr. This figure is based upon data from Hays *et al.* (1976).

In spite of the considerable disagreement obtained at large times between the linear approximation (43) and either the exact or approximate non-linear model, in so far as the response to a Heaviside excitation is concerned, the linear model turns out to be quite adequate for present purposes as shown in the next section.

4 Polar wander for realistic surface load histories

The best currently available data which provide information on the actual time dependence of the extent of northern hemisphere ice coverage are the time series of oxygen isotope variability (O^{16}/O^{18}) obtained for sedimentary cores taken in the deep ocean basins (e.g. Hays, Imbrie & Shackleton 1976). These proxy data, an example of which is shown in Fig. 4, have clearly established the existence of a dominant 10^5yr cycle in the ice coverage record with statistically significant variability also at the periods of 23 000 and 41 000 yr corresponding to the time-scales of the precession of the equinoxes and of changes in orbital obliquity. Although the latter periods are those predicted by the astronomical theory of the ice ages due to Milankovitch, the reason why the 10^5yr fluctuation should so strongly dominate the variability is presently unknown; indeed such variation should not exist according to current elaborations of the Milankovitch hypothesis. From the oxygen isotope data we see that although the accretion and distintegration of the ice sheets is roughly periodic with a period of about 10^5yr, the time-scale of accretion is very much longer than the time-scale of disintegration, leading us to expect that a reasonable approximation to the actual history of loading and unloading might be the sawtooth wave form shown in Fig. 5 (bottom) with a disintegration time of 10^4yr compared to an accretion time of 9×10^4yr.

Here we are interested in fitting the model to the ILS data shown in Fig. 1, which clearly pertains to a time following a major deglaciation episode. We will first establish that the errors incurred in employing the linear model (47) are within tolerable bounds and then proceed to use this linear approximation to infer mantle viscosity from the observed speed of polar wander. An upper bound to the error incurred by making the linear approximation will be obtained by replacing the sawtooth waveform in Fig. 5 by a square wave of the same period, since this will accentuate the effect of non-linearity. For a single 'top hat' glaciation–deglaciation event the speed of polar wander obtained from (47), neglecting the Chandler pole completely, is

$$V(t) = \frac{-\Omega\gamma}{A\sigma_0}(P_1\bar{\mu} - P_2)[\![\exp(-\gamma t) - \exp[-\gamma(t-t^*]]\!], \qquad t > t^* \tag{50}$$

where the constant load is applied at $t = 0$ and removed at $t = t^*$. We compared the linear speed history (50) to that obtained by solving the non-linear system (48) using the excitation function given in Appendix C. For this calculation the duration of the loading event was

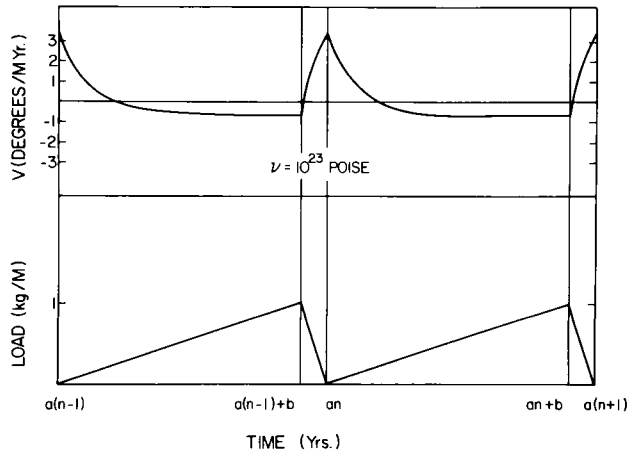

Figure 5. The top frame shows the speed of polar wander as a function of time which is forced by the glaciation–deglaciation history shown in the bottom frame. The triangular wave shape chosen for the loading history is based upon the oxygen isotope data shown in Fig. 4.

fixed at 5×10^4yr, the angular radius of the ice sheet was taken as $\alpha = 15°$, the colatitude of the centre of the ice sheet as 25°, and its mass as 1.8×10^{19}kg. All of these parameters are appropriate approximations for the Laurentide ice sheet (e.g. Peltier *et al.* 1978). As expected, non-linear effects are strongest just after unloading. However, the relative error between the two predictions is at most on the order of 3 per cent and this obtains for the lower value of mantle viscosity, $\nu \sim 10^{22}$poise. It seems clear, on the basis of this comparison, that the linear solution may be safely employed to predict the speed of polar wander following a deglaciation event.

The fairly realistic ramp shaped history shown at the bottom of Fig. 5 has the simple mathematical representation

$$\begin{aligned} F_n(t) &= \frac{t - a(n-1)}{b} && \text{for } a(n-1) < t < a(n-1) + b \\ &= \frac{an - t}{a - b} && \text{for } a(n-1) + b < t < an \end{aligned} \tag{51}$$

for the nth ramp in the time domain (where $n = 1, 2, \ldots,$ etc.). The Laplace transform of $F(t)$ is required in the transform domain representation of the linear solution (47) and is given by

$$\begin{aligned} f_n(s) = \frac{1}{bs^2} &\{\exp[-a(n-1)s] - \exp[\![-[a(n-1)+b]s]\!]\} \\ &- \frac{1}{(a-b)s^2}\{\exp[\![-[a(n-1)+b]s]\!] - \exp(-ans)\} \end{aligned} \tag{52}$$

for the nth ramp in the sequence, with $a = 10^5$yr and $b = 9 \times 10^4$yr in Fig. 5 (these parameters will later be varied to illustrate the dependence of the solution upon them). When (52) is inserted into (47) and the Laplace inverse computed (neglecting the wobble component) we obtain the following analytic expression for the contribution to the speed of

polar wander from the nth load cycle in the time domain as

$$V_n(t) \simeq \frac{\sigma_r}{\sigma_0}\,[V_n^1(t) + V_n^2(t) + V_n^3(t) + V_n^4(t)] \tag{53a}$$

where

$$V_n^1(t) = \gamma\left(\frac{P_1(1+\bar{\mu})}{C-A}\right)\left\{\frac{[t-a(n-1)]}{b}\,[\![H[t-a(n-1)]-H[t-a(n-1)-b]]\!]\right.$$
$$\left.+\frac{(an-t)}{a-b}\,[\![H[t-a(n-1)-b]-H(t-an)]\!]\right\} \tag{53b}$$

$$V_n^2(t) = -\frac{1}{b}\cdot\left(\frac{P_1\bar{\mu}-P_2}{C-A}\right)[\![1-\exp\,[-\gamma(t-a(n-1)]]\!]H[t-a(n-1)] \tag{53c}$$

$$V_n^3(t) = \frac{a}{b(a-b)}\left(\frac{P_1\bar{\mu}-P_2}{C-A}\right)[\![1-\exp\,[-(t-a(n-1)-b]]\!]H[t-a(n-1)-b] \tag{53d}$$

$$V_n^4(t) = -\frac{1}{a-b}\left(\frac{P_1\bar{\mu}-P_2}{C-A}\right)[\![1-\exp\,[-\gamma(t-an)]]\!]H(t-an). \tag{53e}$$

The first term in (53a) is simply the load history itself weighted by the factor $(\sigma_r/\sigma_0)\cdot P_1(1+\bar{\mu})\gamma/(C-A)$, while the three remaining terms contain the relaxation effects. Due to the latter, in any given load cycle the system posesses a memory of all proceeding cycles which must be taken into account. How rapidly the memory fades depends upon the magnitude of the viscosity such that the higher the viscosity the longer the memory. At a particular time t within the nth cycle the contribution of the relaxation terms for the $(n-1)$st cycle is, from (53)

$$V_{n-1}(t) \simeq \frac{\sigma_r}{\sigma_0}\left(\frac{P_1\bar{\mu}-P_2}{C-A}\right)\left(\frac{1}{(a-b)}-\frac{a}{b(a-b)}\exp\,[-\gamma(a-b)]+\frac{1}{b}\exp\,(-\gamma a)\right)$$
$$\times\exp\,[\![-\gamma\,[t-a(n-1)]]\!]. \tag{54}$$

It is therefore clear that the contribution from the $(n-2)$nd cycle will be a factor $\exp(-\gamma a)$ smaller than the contribution from the $(n-1)$st cycle and so on. With $\nu = 10^{23}$ poise, $a\gamma \sim 10$ and a very small error is made if we take into account only the contribution from the immediately preceding cycle. For higher viscosities, a better approximation can be obtained by multiplying (56) by the factor $[1+\exp(-a\gamma)+\exp(-2a\gamma)]$. The speed in the interval $[a(n-1), a(n-1)+b]$ is then obtained by summing (55) and (56) to get

$$V(t) \simeq \frac{\sigma_r}{\sigma_0}\left[\!\!\left[\frac{P_1(1+\bar{\mu})\gamma}{(C-A)}\,\frac{[t-a(n-1)]}{b}+\left(\frac{P_1\bar{\mu}-P_2}{(C-A)}\right)\right.\right.$$
$$\left.\left.\times\left[\left(\frac{a}{b(a-b)}\,[\![1-\exp\,[-\gamma(a-b)]]\!]+\frac{1}{b}\exp\,(-\gamma a)\right)\exp\,[\![-\gamma\,[t-a(n-1)]]\!]-\frac{1}{b}\right]\right]\!\!\right] \tag{55}$$

while in the interval $[a(n-1)+b, an]$ it is the sum of the term in square brackets in (55) and

$$V(t) \simeq \frac{\sigma_r}{\sigma_0}\left[\frac{P_1(1+\bar{\mu})\gamma}{(C-A)}\,\frac{(an-t)}{(a-b)}+\left(\frac{P_1\bar{\mu}-P_2}{C-A}\right)\frac{a}{b(a-b)}\left\{1-\exp\,[\![-\gamma\,[t-a(n-1)-b]\,]\!]\right\}\right]. \tag{56}$$

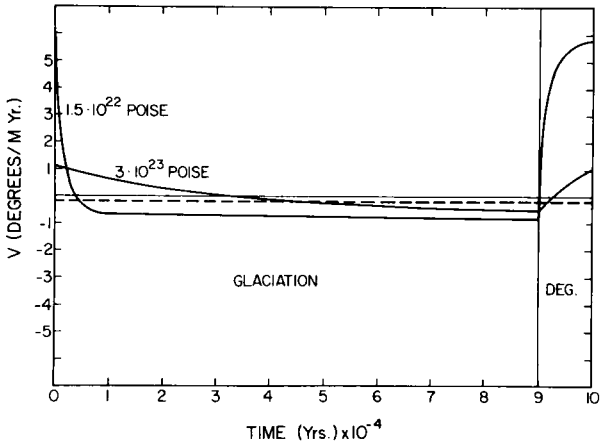

Figure 6. Speed of polar wander as a function of time during the periodic glaciation–deglaciation history shown in Fig. 7. Solutions for different values of the viscosity are as marked and the dashed line denotes the average speed for the case $\nu = 1.5 \times 10^{22}$ poise.

As a matter of convention, in the following figures the speed of polar wander is taken positive when the direction of motion is towards the region that is glaciated. In Fig. 6 we show the speed of polar wander as a function of time for different values of the viscosity of the mantle when the excitation uses the previously stated values of the parameters appropriate to the Laurentide ice sheet. Within the range of viscosities which concerns us, the relaxation terms do not contribute to the *average* speed. This turns out to be equal to the instantaneous speed obtained above for the box-shaped load history if an ice sheet mass equal to half that employed in the realistic history is used. This average speed is

$$\bar{V} = \frac{\Omega\gamma}{A\sigma_0} P_1 \frac{(1+\bar{\mu})}{2} \tag{57}$$

and this is also shown by the dashed line on Fig. 6 for the lower viscosity model. From Fig. 6 it is clear that the higher the value of the viscosity the smaller are the fluctuations of the instantaneous speed about the average value. In Fig. 7 we show the same variability as a

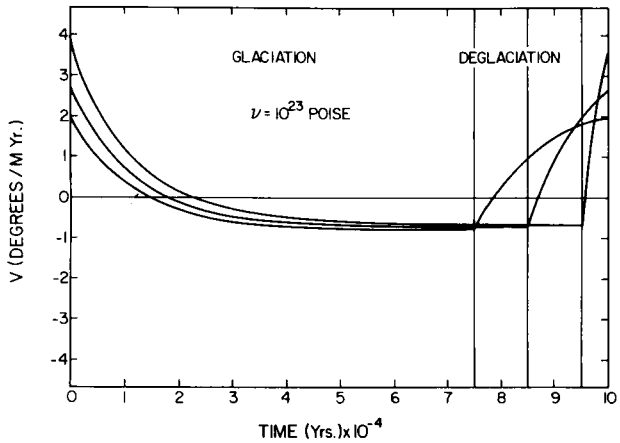

Figure 7. Same as in Fig. 8 but for different values of the deglaciation time-scale b.

function of the relative durations of the glaciation and deglaciation parts of the loading cycle. The more rapid the deglaciation the higher the instantaneous speed following the event. As $a - b$ tends to zero, the values of the speed in the two limits $t \to an^-$ and $t \to an^+$ do not match and we get a discontinuity as in the case of the box-shaped history. Another fact which we must draw attention to here, is that the average speed of polar wander does not depend upon the details of the load history within the cycle.

The average speed (57), deduced from linear theory, is of course invariant from cycle to cycle and this cannot be correct because, as demonstrated explicitly in Section 3, the speed of wander decreases as the system approaches equilibrium (see Fig. 3). This variation is determined by the non-linearity of the system. Since the present configuration of the system is quite far from equilibrium (given the geographic location of the main loading event) it is clear that linear theory should be rather accurate as a description of the currently continuing polar wander.

In order to compare the predictions of the model with the ILS data shown in Fig. 1 we shall assume that the instantaneous measurement of the speed of polar wander which these data provide corresponds to a time of hiatus in a previously continuous loading–unloading cycle. In this case $V(t)$ predictions from the time of the last unloading event are shown in Fig. 8 for representative values of viscosity on the basis of equation (54). In constructing this figure we have assumed that the centre of the 10^4 yr deglaciation period of the ramp-shaped model corresponds to a time 8000 yr ago since this gives a best fit to the glacial chronology in Peltier & Andrews (1976). Superimposed upon the $V(t)$ curve is the speed of polar wander implied by the ILS–IPMS data of about $1^0/10^6$ yr and the errors associated with this inference given by Dickman (1977). It is quite clear by inspection of this figure that we can fit the observation with our deglaciation-induced polar wander model either with a low mantle viscosity of about 1.5×10^{22} poise or with a relatively high value of (say) 3×10^{23} poise. With allowance for timing errors and geographic effects not included in the model we cannot exclude any viscosity within some range of each of the extreme values if we employ only the single observation of polar wander speed to constrain the parameter. We expect, for example, that proper incorporation of the effect of the Fennoscandian load into the model

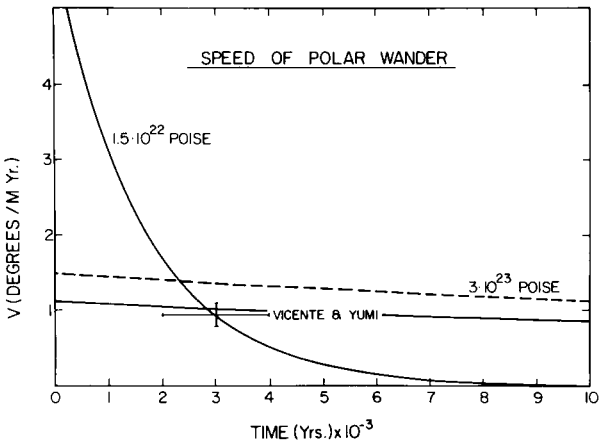

Figure 8. Speed of polar wander following the last deglaciation event under the assumption that the system is not currently glaciating. The observation (from Fig. 1) may be fit with either of the two different values of the viscosity shown. The dashed line is the prediction from the 3×10^{23} poise model under the assumption that the system is in isostatic equilibrium before deglaciation begins and illustrates the importance of the load history in this case. For the 1.5×10^{22} poise model this assumption leads to no significant difference in the prediction.

and allowance for the radial heterogeneity of the Earth will lower the largest allowed viscosity from 3×10^{23} poise to somewhat less than 10^{23} poise.

The dashed line on Fig. 8 illustrates the variation of the speed of polar wander predicted when we account only for the unloading part of the glacial cycle. In this case the speed prediction is simply

$$V^*(t) \simeq \frac{\sigma_r}{\sigma_0} \cdot \left(\frac{P_1\bar{\mu} - P_2}{C - A}\right)\left(\frac{1}{a - b}\right) [\![1 - \exp[-\gamma(a-b)]]\!] \exp[\![-\gamma[t - a(n-1)]]\!] \qquad (58)$$

$$t > a(n-1)$$

which is obtained under the assumption that prior to the onset of deglaciation the load is in isostatic equilibrium. As is apparent by inspection of Fig. 8, the speed in this case is considerably overestimated for the high viscosity model with $\nu = 3 \times 10^{23}$ poise (by approximately 30 per cent). With viscosity $\nu \sim 10^{22}$ poise the memory is much shorter and the predictions $V(t)$ and $V^*(t)$ nearly coincide. This result serves to demonstrate that if the higher value of the viscosity is most appropriate then the load history may have an appreciable impact on the estimate of viscosity which we obtain by fitting the model to observations.

The results obtained in this section very clearly demonstrate that the polar wander component of the ILS–IPMS pole path is just that expected to exist as a consequence of the disintegration of the large Pleistocene ice masses if the Earth has the viscosity structure which is required to fit postglacial rebound data (Peltier 1980; Peltier *et al.* 1978). The two analyses are therefore mutually reinforcing. This interpretation of the source of the secular trend in the polar motion data is different from a commonly held idea that the polar wander implied by these data is a consequence of changes in inertia associated with continental drift. Dickman (1977, 1979), making use of the plate velocity model proposed by Minster *et al.* (1974), found that such effects could not explain any substantial portion of the secular motion. Even under the most favourable circumstances, and by comparing plate velocity models of Solomon, Sleep & Richardson (1975), Kaula (1975) and Minster *et al.* (1974), continental drift could account for no more than about 30 per cent of the observed speed (the direction of motion not withstanding). A similar estimate has been obtained by Yumi & Wako (1968) who based their analysis on the local residuals at each ILS station. The observed mean polar motion appears to be forced by Pleistocene deglaciation.

In our analysis of polar wander we have completely ignored the excitation of Chandler wobble by the time-dependent surface mass load. That this assumption is reasonable can be seen from (47) in which it is clear that the efficiency of excitation of the Chandler mode depends on the energy in the excitation function $\phi(s)$ at the Chandler frequency $s = i\sigma_0$. Since the 'realistic' load history employed in this section artificially reduces the high-frequency forcing by assuming a regular sawtooth history with a 10^5 yr period, we must reconsider the loading model in order to obtain a realistic estimate of the forced Chandler amplitude. Evidence of high-frequency structure within the last 10^5 yr cycle has been presented recently in Andrews & Barry (1978) in which it is suggested that during the accretion period there were superimposed fluctuations in global sea-level of 30–60 m at rates of 2–6 m/10^3 yr (their fig. 2). If we use our triangular pulse model to compute the forced wobble amplitude from (47) for such excitation, using $a - b = a^*$ and $a = 2a^*$ in the excitation function, then we obtain the wobble amplitude $A(a^*) = (1/a^*)[(P_1 + P_2)/(C - A)] \cdot |\sigma_r/(\gamma - i\sigma_0)^2|$. Even under the most favourable circumstances discussed by Andrews & Barry, we can expect, from this, a wobble amplitude no greater than about 0.002″ and this is completely negligible compared to that which we observe to be forced by earthquake and meteorological excitations.

In the next section we employ our model to make predictions of non-tidal lod variations and to compare these predictions with observation. This will provide a second means of estimating mantle viscosity from polar motion data. As we will show, this estimate coincides with that just obtained by fitting the same model to the observed polar wander.

5 Length of day variations produced by deglaciation

Within the framework of the linear approximation employed in the last section, variations in lod in the coordinate system $Ox_1x_2x_3$ may be obtained in the time domain by means of the relation (Munk & MacDonald 1960)

$$\frac{dm_3}{dt} = \frac{d\phi_3}{dt} \tag{59}$$

where ϕ_3 is obtained from the change in the moment of inertia about the x_3 axis (I_{33}) via equation (46), which is itself obtained in the Laplace transform domain by rotating I'_{ij} (one component of which is given in (35)) into the $Ox_1x_2x_3$ system. From this we obtain the Laplace transform of $\phi_3(t)$ as

$$\begin{aligned}\mathscr{L}[\phi_3(t)] = s\phi_3(s) = -\frac{1}{C}\left(\frac{1-3\cos^2\theta}{3\cos\theta\sin\theta}\right)\left[P_1\left(1+\frac{\bar{\mu}\gamma}{s+\gamma}\right)+\frac{P_2 s}{s+\gamma}\right] \\ \times\left(\frac{1}{bs}\left\{\exp\left[-a(n-1)s\right]-\exp\left[\!\left[-\left[a(n-1)+b\right]s\right]\!\right]\right\}\right. \\ \left.-\frac{1}{(a-b)s}\left\{\exp\left[\!\left[-\left[a(n-1)+b\right]\right]\!\right]-\exp\left(-ans\right)\right\}\right)\end{aligned} \tag{60}$$

when the spectrum (52) is employed. In the time domain (60) gives

$$\frac{dm_3(t)}{dt} = -\left(\frac{1-3\cos^2\theta}{3\cos\theta\sin\theta}\right)\left[\Upsilon^1(t)+\Upsilon^2(t)+\Upsilon^3(t)\right] \tag{61a}$$

where

$$\begin{aligned}\Upsilon^1(t) = \left(\frac{P_1(1+\bar{\mu})}{C}\right)\left(\frac{1}{b}\left[\!\left[H\left[t-a(n-1)\right]-H\left[t-a(n-1)-b\right]\right]\!\right]-\frac{1}{a-b}\right. \\ \left.\times\left[\!\left[H\left[t-a(n-1)-b\right]-H(t-an)\right]\!\right]\right)\end{aligned} \tag{61b}$$

$$\begin{aligned}\Upsilon^2(t) = \frac{1}{b}\left(\frac{P_2-P_1\bar{\mu}}{C}\right)\left\{\exp\left[\!\left[-\gamma\left[t-a(n-1)\right]\right]\!\right]H\left[t-a(n-1)\right]-\exp\left[\!\left[-\gamma\left[t-a(n-1)\right.\right.\right.\right. \\ \left.\left.\left.\left.-b\right]\right]\!\right]H\left[t-a(n-1)-b\right]\right\}\end{aligned} \tag{61c}$$

$$\begin{aligned}\Upsilon^3(t) = -\frac{1}{a-b}\left(\frac{P_2-P_1\bar{\mu}}{C}\right)\left\{\exp\left[\!\left[-\gamma\left[t-a(n-1)-b\right]\right]\!\right]H\left[t-a(n-1)-b\right]\right. \\ \left.-\exp\left[-\gamma(t-an)\right]H(t-an)\right\}, \qquad t\in[a(n-1),\ an]\end{aligned} \tag{61d}$$

and $n = 1, 2, \ldots$, etc. When $t > a(n-1)$ the contribution from the $(n-1)$st ramp is given by (61) with n replaced by $n-1$ and the constant term dropped, i.e.

$$\frac{dm_3}{dt} = \frac{-1}{C}\left(\frac{1-3\cos^2\theta}{3\sin\theta\cos\theta}\right)\left(\frac{(P_2 - P_1\bar{\mu})}{(a-b)}\,[\![1-\exp[-\gamma(a-b)]]\!]\right.$$
$$\left. + \frac{(P_1\bar{\mu} - P_2)}{b}\,[1-\exp(-\gamma b)]\exp[-\gamma(a-b)]\right)\exp[\![-\gamma[t-a(n-1)]]\!]. \qquad (62)$$

Equation (62) may be integrated to obtain the logarithmic derivative of $m_3(t)$ which is required for comparison with observations. In Fig. 9 we plot two histories of $\dot{m}_3/m_3$ for different values of the mantle viscosity, with all other parameters of the model fixed as in the last section. As in the previous discussion of polar wander we have included in the calculations shown on Fig. 9, effects due to the two previous load cycles by multiplying (62) by the factor $[1+\exp(-a\gamma)+\exp(-2a\gamma)]$. Clearly, even for $\nu = 3\times10^{23}$ poise, the influence of the earliest of these previous cycles is negligible. The observational data shown on Fig. 9 warrant some comment. Besides the vertical error bars associated with the acceleration measurement itself, we have affixed horizontal error bars to account for errors in timing. As previously, in plotting the data we have assumed that the midpoint of the final deglaciation stage corresponds to a time 8000 yr before present. The slight temporal displacements of the different observations shown on Fig. 9 have been introduced solely for convenience in plotting and have no physical basis. The observation labelled C is based on the analysis by Currot (1966) and is consistent with that of Dicke (1966). The data labelled M & S is from Muller & Stephenson (1975) who re-analysed the ancient eclipse data employed by Newton (1972) keeping only those corresponding to total solar eclipses or for which deviation from totality was explicitly declared. The value marked M was obtained by Morrison (1973) based upon lunar occulations over the period 1663–1972. This observation deviates significantly from the others and may be strongly biased by long-period fluctuations in the Earth's acceleration since the observation period is rather short. The value marked L was proposed by Lambeck (1977) and was obtained from the difference between the value of the acceleration given by Muller (1975) and the mean of the Earth's tidal acceleration obtained from an ocean model and astronomical and satellite observations.

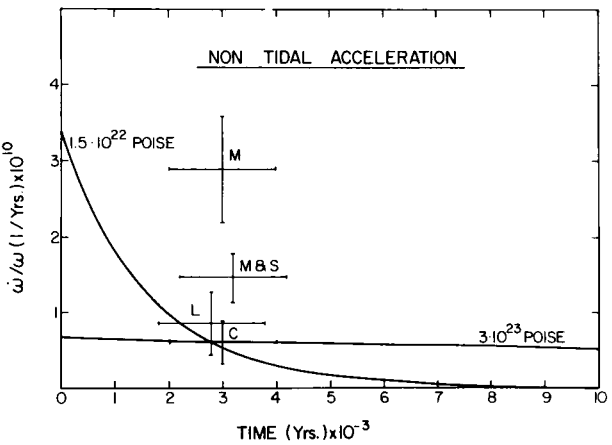

Figure 9. Non-tidal acceleration of the length of day (lod) following the last deglaciation event for the two different viscosity models which fit the data. Observations are from Currot (C), Morrison (M), Muller & Stephenson (M & S) and Lambeck (L).

Assuming Morrison's data to be unreliable, we see from Fig. 9 that our model fits the data for either of two quite widely separated values of the mantle viscosity; in fact, with precisely the same range of values found from the polar wander data. Therefore, the same ambiguity of interpretation exists in the case of the analysis of lod variations as found previously. From the two acceptable values of mantle viscosity ($\sim 1.5 \times 10^{22}$ poise and $\sim 3 \times 10^{23}$ poise) we have two possible relaxation times for the $l = 2$ harmonic of $\sim 1.5 \times 10^3$ yr and $\sim 3 \times 10^4$ yr. This ambiguity was pointed out in past work on lod data by both O'Connell (1971) who quoted relaxation times of 2×10^3 yr and 10^5 yr and Lambeck (1975) who found acceptable relaxation times of either 4×10^3 yr or 4×10^4 yr.

6 Conclusions

On the basis of the preceding analysis it seems clear to us that both the currently observed polar wander and the non-tidal lod variation are a consequence of forcing due to the build-up and disintegration of the large northern hemisphere ice sheets which has taken place quasi-periodically during the present glacial epoch. Both these observed polar motions are precisely those which are expected if the viscosity of the mantle has a mean value compatible with the postglacial rebound data. The two types of analysis, rebound and polar motion, are therefore mutually reinforcing. In the analysis of polar motion discussed in this paper we have employed an homogeneous earth model and a simplified deglaciation history. Because of the homogeneity of the model, the viscosity inferred by fitting it to the data must be interpreted as a mean mantle viscosity. Since the rebound data require an upper mantle viscosity of 10^{22} poise with an increase to a value of about 10^{23} poise in the lower mantle, the mean will be dominated by the lower mantle viscosity to which the $l = 2$ harmonic which governs the polar motion is extremely sensitive. The fact that the polar motion depends only on the response of the $l = 2$ harmonic also ensures that the simple approximation for the ice sheet geometry which we have employed will introduce no appreciable error into the analysis. Although this simplified analysis deserves to be repeated using the full apparatus for inhomogeneous viscoelastic models developed in Peltier (1974) and using a more fully realistic deglaciation history as described in Peltier & Andrews (1976) for example, we do not expect that this increase in sophistication of the model will lead to any substantial change in the interpretation of the polar motion data. These data are extremely important in that they enable us to obtain a strong upper bound on the viscosity of the mantle beneath the transition region. This viscosity is not sufficiently high as to inhibit the whole mantle mode of convection.

Acknowledgments

The research reported in this paper was conducted during the research leave of R. Sabadini who was financed by E. Boschi through the Progetto Finalizzato Geodinamica. We wish to acknowledge useful discussions with Patrick Wu and David Yuen during the course of the work, and support through NSERCC Grant A-9627.

References

Andrews, J. T. & Barry, R. G., 1978. Glacial inception and disintegration during the last glaciation, *Ann. Rev. Earth planet. Sci.*, **6**, 205–228.

Burgers, J. M., 1955. Rotational motion of a sphere subject to visco-elastic deformation. I, II, III, *Proc. K. ned. Akad. Wet.*, **58**, 219–237.

Currot, D. R., 1966. Earth deceleration from ancient solar eclipses, *Astr. J.*, **71**, 264–269.

Dicke, R. H., 1966. The secular acceleration of the Earth's rotation and cosmology, in *The Earth–Moon System*, pp. 98–163, eds Marsden, B. G. & Cameron, A. G. W., Plenum Press, New York.

Dickman, S. R., 1977. Secular trend of the Earth's rotation pole: consideration of motion of the latitude observatories, *Geophys. J. R. astr. Soc.*, **51**, 229–244.

Dickman, S. R., 1979. Continental drift and true polar wandering, *Geophys. J. R. astr. Soc.*, **57**, 41–50.

Enright, W. H. & Hull, T. E., 1976. Test results on initial value methods for non-stiff ordinary differential equations, *Siam J. Numer. Anal.*, **13**, 944–961.

Farrell, W. E., 1972. Deformation of the earth by surface loads, *Rev. Geophys. Space Phys.*, **10**, 761–797.

Goldstein, H., 1950. *Classical Mechanics*, Addison-Wesley, Cambridge, Massachusetts.

Hays, J. D., Imbrie, J. & Shackleton, N. J., 1976. Variations in the earth's orbit: pacemaker of the Ice Ages, *Science*, **194**, 1121–1132.

Jeffreys, H., 1970. *The Earth*, 4th edn, Cambridge University Press, London.

Kaula, W. M., 1975. Absolute plate motions by boundary velocity minimizations, *J. geophys. Res.*, **80**, 244–248.

Lambeck, K., 1975. Effects of tidal dissipation in the oceans on the Moon's orbit and the Earth's rotation, *J. geophys. Res.*, **80**, 2917–2925.

Lambeck, K., 1977. Tidal dissipation in the oceans: astronomical, geophysical and oceanographic consequences, *Phil. Trans. R. Soc. A*, **287**, 545–594.

Minster, J. B., Jordan, T. H., Molnar, P. & Haines, E., 1974. Numerical modelling of instantaneous plate tectonics, *Geophys. J. R. astr. Soc.*, **36**, 541–576.

Morrison, L. V., 1973. Rotation of the earth and the constancy of *G*, *Nature*, **241**, 519–520.

Muller, P. M., 1975. An analysis of the ancient astronomical observations with the implications for geophysics and cosmology, *thesis*, University of Newcastle.

Muller, P. M. & Stephenson, F. R., 1975. The acceleration of the Earth and Moon from early observations, in *Growth Rhythms and History of the Earth's Rotation*, pp. 459–534, eds Rosenberg, G. D. & Runcorn, S. K., Wiley, New York.

Munk, W. H. & MacDonald, G. J. F., 1960. *The Rotation of the Earth*, Cambridge University Press.

Newton, R. R., 1972. *Medieval Chronicles and the Rotation of the Earth*, Johns Hopkins University Press, Baltimore.

O'Connell, R. J., 1971. Pleistocene glaciation and the viscosity of the lower mantle, *Geophys. J. R. astr. Soc.*, **23**, 299–327.

Peltier, W. R., 1974. The impulse response of a Maxwell earth, *Rev. Geophys. Space Phys.*, **12**, 649–669.

Peltier, W. R., 1976. Glacial-isostatic adjustment – II. The inverse problem, *Geophys. J. R. astr. Soc.*, **46**, 669–705.

Peltier, W. R., 1980. Mantle convection and viscosity, in *Physics of the Earth's Interior*, eds Dziewonski, A. & Boschi, E., Elsevier-North Holland, New York.

Peltier, W. R. & Andrews, J. T., 1976. Glacial isostatic adjustment – I. The forward problem, *Geophys. J. R. astr. Soc.*, **46**, 605–646.

Peltier, W. R., Farrell, W. E. & Clark, J. A., 1978. Glacial isostasy and relative sea level: a global finite element model, *Tectonophys.*, **50**, 81–110.

Rochester, M. G. & Smylie, D. E., 1974. On changes in the trace of the earth's inertia tensor, *J. geophys. Res.*, **79**, 4948–4951.

Shepard, F. P., 1963. Thirty-five thousand years of sea level, *Essays in Marine Geology*, pp. 1–10, University of Southern California Press.

Solomon, S. C., Sleep, N. H. & Richardson, R. M., 1975. On the forces driving plate tectonics: inferences from absolute plate velocities and intra-plate stress, *Geophys. J. R. astr. Soc.*, **42**, 769–801.

Vicente, R. O. & Yumi, S., 1969. Co-ordinates of the pole (1899–1968), referred to the conventional international origin, *Publs int. Latit. Obs. Mizusawa*, **7**, 41–50.

Vicente, R. O. & Yumi, S., 1970. Revised values (1941–1961) of the co-ordinates of the pole referred to the CIO, *Publs int. Latit. Obs. Mizusawa*, **7**, 109–112.

Wu, P. & Peltier, W. R., 1981a. Viscous gravitational relaxation, *Geophys. J. R. astr. Soc.*, submitted.

Wu, P. & Peltier, W. R., 1981b. Glacial isostatic adjustment and the free air gravity anomaly as a constraint on deep mantle viscosity, *Geophys. J. R. astr. Soc.*, submitted.

Yumi, S. & Wako, Y., 1968. On the secular motion of the mean pole, in *Continental Drift, IAU Symp. 32*, pp. 33–36, eds Markowitz, W. & Guinot, B., Reidel, Dordrecht, Holland.

Appendix A

In this section the previously defined parameter R is normalized by dividing by the inertia I defined in equation (13). With this modification, the components of the symmetric matrix $\mathbf{A}^*$, in non-dimensional form, are

$$A^*_{11} = 1 + \frac{2}{3} R(3y_1^2 + y_2^2 + y_3^2) - R\frac{\bar{\mu}}{3} \exp\left[-(\gamma/\Omega R\bar{\mu})x\right] - R\frac{\bar{\mu}}{3}(-2y_4 + y_5 + y_6)$$

$$A^*_{12} = \frac{4}{3} R y_1 y_2 + R\bar{\mu} y_7$$

$$A^*_{13} = \frac{4}{3} R y_1 y_3 + R\bar{\mu} y_8$$

$$A^*_{22} = 1 + \frac{2}{3} R(y_1^2 + 3y_2^2 + y_3^2) - R\frac{\bar{\mu}}{3} \exp\left[-(\gamma/\Omega R\bar{\mu})x\right] - R\frac{\bar{\mu}}{3}(y_4 - 2y_5 + y_6)$$

$$A^*_{23} = \frac{4}{3} R y_2 y_3 + R\bar{\mu} y_9$$

$$A^*_{33} = 1 + \frac{2}{3} R(y_1^2 + y_2^2 + 3y_3^2) + \frac{2}{3} R\bar{\mu} \exp\left[-(\gamma/\Omega R\bar{\mu})x\right] - R\frac{\bar{\mu}}{3}(y_4 + y_5 - 2y_6).$$

The components of the matrix $\mathbf{B}^*$, in non-dimensional form, are

$$B^*_{11} = -\frac{\gamma}{3\Omega}\left[\!\left[\exp\left[-(\gamma/\Omega R\bar{\mu})x\right] - 2y_4 + y_5 + y_6\right]\!\right] - \frac{2\gamma}{3\Omega}(y_1^2 + y_2^2 + y_3^2)$$

$$B^*_{12} = \frac{\gamma}{\Omega} y_7 - \exp\left[-(\gamma/\Omega R\bar{\mu})x\right] y_3 - (y_1 y_8 + y_2 y_9 + y_3 y_6)$$

$$B^*_{13} = \frac{\gamma}{\Omega} y_8 + y_1 y_7 + y_2 y_5 + y_3 y_9$$

$$B^*_{21} = \frac{\gamma}{\Omega} y_7 + \exp\left[-(\gamma/\Omega R\bar{\mu})x\right] y_3 + y_1 y_8 + y_2 y_9 + y_3 y_6$$

$$B^*_{22} = -\frac{\gamma}{3\Omega}\left[\!\left[\exp\left[-(\gamma/\Omega R\bar{\mu})x\right] + y_4 - 2y_5 + y_6\right]\!\right] - \frac{2\gamma}{3\Omega}(y_1^2 + y_2^2 + y_3^2)$$

$$B^*_{23} = \frac{\gamma}{\Omega} y_9 - (y_1 y_4 + y_2 y_7 + y_3 y_8)$$

$$B^*_{31} = \frac{\gamma}{\Omega} y_8 - (y_1 y_7 + y_2 y_5 + y_3 y_9)$$

$$B^*_{32} = \frac{\gamma}{\Omega} y_9 + y_1 y_4 + y_2 y_7 + y_3 y_8$$

$$B^*_{33} = \frac{\gamma}{3\Omega}\left[\!\left[2\exp\left[-(\gamma/\Omega R\bar{\mu})x\right] - y_4 - y_5 + 2y_6\right]\!\right] - \frac{2\gamma}{3\Omega}(y_1^2 + y_2^2 + y_3^2).$$

The only non-zero components of the matrix **D** are the following

$$D_{ii} = -\frac{\gamma}{\Omega R\bar{\mu}}, \quad i = 4\text{–}9$$

$$D_{41} = \frac{\gamma}{\Omega R\bar{\mu}}\, y_1$$

$$D_{52} = D_{71} = \frac{\gamma}{\Omega R\bar{\mu}}\, y_2$$

$$D_{63} = D_{81} = D_{92} = \frac{\gamma}{\Omega R\bar{\mu}}\, y_3.$$

Appendix B

The matrix **P** is defined in the following way

$$\mathbf{P} = g(x)\begin{bmatrix} a & 0 & c \\ 0 & 1 & 0 \\ c & 0 & b \end{bmatrix} \tag{B1}$$

where

$$a = 1 - 3\sin^2\theta, \quad b = 1 - 3\cos^2\theta, \quad c = 3\cos\theta\sin\theta,$$

and $g(x)$ is defined as follows when the time history of the load is a step function

$$g(x) = \left(\frac{a^2 L_2}{3I}\right)\left[l + \frac{\mu}{1+\bar{\mu}}\right](1-l)\exp\left[-(\gamma/\Omega R\bar{\mu})x\right]. \tag{B2}$$

In the following

$$d(x) = \frac{d}{dx}\, g(x). \tag{B3}$$

The components of the matrix **Q** are given by

$$Q_{11} = -\frac{\gamma}{\Omega R\bar{\mu}} \cdot a\, d(x)$$

$$Q_{12} = -\frac{c}{R\bar{\mu}}\, g(x) y_1 - \frac{b-1}{R\bar{\mu}}\, g(x) y_3$$

$$Q_{13} = -\frac{\gamma}{\Omega R\bar{\mu}}\, c\, d(x)$$

$$Q_{21} = \frac{c}{R\bar{\mu}}\, g(x) y_1 + \frac{b-a}{R\bar{\mu}}\, g(x) y_3$$

$$Q_{22} = -\frac{\gamma}{\Omega R\bar{\mu}}\, d(x)$$

$$Q_{23} = -\frac{c}{R\bar{\mu}}\, g(x) y_3$$

$$Q_{31} = -\frac{\gamma}{\Omega R\bar{\mu}}\, cd(x) + \frac{a-1}{R\bar{\mu}}\, g(x) y_2$$

$$Q_{32} = \frac{c}{R\bar{\mu}}\, g(x) y_3$$

$$Q_{33} = -\frac{\gamma}{\Omega R\bar{\mu}}\, bd(x).$$

Appendix C

The quantities Γ, S_1, S_2, S_3 entering the set of equations (50) are defined as

$$\Gamma = \frac{\Omega(C-A)\bar{\mu}}{C(1+\bar{\mu})\gamma} \tag{C1}$$

$$S_1(x) = \frac{\Omega \cdot \mathrm{SCALE}}{1+\Gamma^2}\,[(1-b)m_2 m_3 - cm_1 m_2]g(x)$$

$$S_2(x) = \frac{\Omega \cdot \mathrm{SCALE}}{1+\Gamma^2}\,[(b-a)m_1 m_3 + c(m_1^2 - m_3^2)]g(x) \tag{C2}$$

$$S_3(x) = \frac{\Omega \cdot \mathrm{SCALE}}{1+\Gamma^2}\,[(a-1)m_1 m_2 + cm_2 m_3]g(x)$$

where a, b and c are defined in Appendix B when $g(x)$ corresponds to a step function. After the end of the box as in Section 4, the function $g(x)$ is given by

$$g(x) = \frac{\bar{\mu}}{3(1+\bar{\mu})}\,(l-1)\,\frac{a^2 L^2}{I}\,[\![\exp\,[-\gamma \cdot \mathrm{SCALE}(x-x^*)]\,\exp\,[-\gamma \cdot \mathrm{SCALE}\,x]]\!] \tag{C3}$$

where x^* is the non-dimensional time at which the step load is removed.